Article ID: 1007-7294(2024)12-1953-17

Forming and Springback Prediction of Strips Under Multi-square Punch Concave Forming Process Considering Partial-unloading Effects

LIANG Qi-yu[1,2], *ZHANG Long*[1,2,3], *ZHU Ling*[1,2,3]

(1. Key Laboratory of High Performance Ship Technology (Wuhan University of Technology), Ministry of Education, Wuhan 430063, China; 2. School of Naval Architecture, Ocean and Energy Power Engineering, Wuhan University of Technology, Wuhan 430063, China; 3. Weihai Research Institute of Wuhan University of Technology, Weihai 264309, China)

Abstract: To further investigate the forming mechanism and springback characteristics of strips under multi-square punch forming (MSPF) considering partial-unloading effects, a series of concave forming tests of strips are conducted on the MSPF machine. This paper aims to reveal the physical mechanism of the elastic-plastic deformation in the MSPF process considering the effect of the forming approaches, and derive appropriate mathematical interpretations. The theoretical model is firstly established to analyse the concave forming mechanism and springback characteristics of the strip, and its accuracy is then validated by experimental data. The forming history and load evolutions are depicted to explore the required forming capacity through the proposed analytical method. Besides, the parametric studies are carried out to discuss their effects on the springback of the strip. The results suggest that the deformation paths of the strip are influenced by the forming approach, and the springback of the strip in convex forming is larger than that in concave forming.

Key words: multi-square punch forming (MSPF); follower load; elastic-plastic deformation; partial-unloading; springback prediction

CLC number: U661.4 **Document code:** A **doi:** 10.3969/j.issn.1007-7294.2024.12.011

0 Introduction

In shipbuilding industry, line heating is a practical method for manufacturing hull plates[1], resulting in thermal residual stress. Rigid tools, which are commonly used in aerospace and vehicles, are not economical due to the uniqueness and non-mass production of the hull plate. The flexible multi-point forming method discretizing the rigid tool into small dies that can further form into different shapes, was firstly proposed by some Japanese researchers for plate forming with arbitrary target shape. In 1999, Li et al[2] developed a multi-point forming machine; Wuhan University of Technology cooperated with Shandong Shuoli Machinery Manufacturing Co. Ltd. in developing a three-

Received date: 2024-06-17

Foundation item: Supported by the National Natural Science Foundation of China (52201378) and Open Fund of Weihai Research Institute of Wuhan University of Technology (WHYJY-KJ2021-008)

Biography: LIANG Qi-yu(1993-), female, lecturer; ZHANG Long(2000-), male, master student; ZHU Ling(1962-), male, professor, corresponding author, E-mail: Lingzhu@whut.edu.cn.

dimensional CNC hull plate forming machine in 2010, achieving the multi-point forming (MPF) and multi-square punch forming (MSPF) of the hull plate automatically and economically, respectively[3]. Compared with the MPF, the MSPF overcomes the dimples and wrinkles effectively because the staggered adjustable square heads can establish contact with the plate in a larger area. However, the springback in MSPF is another factor that affects the forming quality of the hull plate. Thus, the accurate springback prediction is of significant importance in hull plate forming with high quality.

There are some experimental and numerical studies about the springback of the MSPF of plates with different target shapes[4-5]. Although these studies have successfully reproduced the springback phenomenon, theoretical interpretations of the mechanics of the springback are rare. In order to investigate the springback in MSPF, the strip or the beam is undoubtedly the most representative research object that can explain the springback mechanism. Yu et al[6] and Zhang et al[7] conducted pioneer researches about the plastic forming of strips on rigid tools both theoretically and experimentally. After that, many researchers studied the large deformation of straight beams or curved beams under a concentrated load at the free end[8] or a uniformly distributed load[9] or a combination of both two[10], aiming to uncover the forming mechanism of strips or beams under different loading conditions. Unlike these loading scenarios, the directions of loads added on the plate in MSPF vary during the process, but they are always normal to the plate at the contact point, just as a particular follower load.

At the very beginning, the concept of follower load was raised in the structural stability analysis in non-conservative system[11], and then applied to the non-linear analyses of cantilevers subjected to different types of follower load by different semi-analytical[12] and numerical methods[13]. As for the closed-form solutions about beams under follower load, Shvartsman analysed a cantilever beam under a concentrated follower force at free end[14], and under two concentrated follower forces at different positions[15], respectively, and solved the elastic deformation of the beam directly. Zhu et al[16] simplified the multi-square punch convex forming process as a cantilevered strip formed by follower loads, and revealed the elastic-perfectly-plastic forming and springback mechanism of the strip theoretically.

In the convex forming scenarios, when the forming curvature of the strip is equal to the curvature of the corresponding position on the lower dies, part of the strip wraps the lower dies and the wrapped part deforms no more until the loading ends. However, the forming curvature at the bottoming point on the strip is larger than the lower die in concave forming, and unloading occurs partially with the forming process going on, which is quite different from the case in convex forming. As the strip slides along the surface constructed by the lower dies, the forming behaviour of the strip is also affected by the bending-under-tension friction[17]. The final state at the end of the forming process, which is dependent on the deformation history, is of great significance in accurate springback prediction[18]. Eggertsen and Mattiasson[19] compared different yielding criteria and hardening laws that can fulfil the requirements concerning accuracy of the springback prediction, and investigated the complexity of the strip's forming through bending-unbending experiments. Pandit and Patel[20] proposed an approach for describing a moment-curvature relationship from any given stress-strain

law, which is very useful in cyclic loading where reverse plastic deformation has occurred.

Thus, on the basis of Ref.[16], a theoretical model of the elastic-perfectly-plastic strip in multi-square punch concave forming will be established in this paper considering the influence of partial unloading during the whole forming process, revealing the forming and springback mechanism of the strip, and discussing the effect of the forming approaches and friction coefficients on the springback of the strip. The rest of the paper will be arranged as following. In Chapter 1, the material properties and the multi-square punch concave forming process of the strip will be introduced briefly. The forming and springback formulae of the elastic-perfectly-plastic strip will be theoretically derived in Chapter 2, while the results calculated by the theoretical model will be validated and parametric studies will be conducted in Chapter 3. Finally, some concluding remarks will be presented in Chapter 4.

1 Experimental procedures and details

1.1 Static tensile tests

Static tensile tests were conducted on the tensile test machine. For each thickness of strips, three standard tensile test specimens were tested. The data obtained directly from the machine were force and displacement corresponding to the engineering stress σ and strain ε. The true stress and true strain were calculated using $\sigma_{true}=\sigma(1+\varepsilon)$, $\varepsilon_{true}=\ln(1+\varepsilon)$. True stress-strain curve of two sample strips with $2t$=5.89 mm and $2t$=11.90 mm are depicted as examples in Fig.1, and the corresponding material properties of these strips are listed in Tab.1 including yield stresses and ultimate stresses according to the true stress-strain curve.

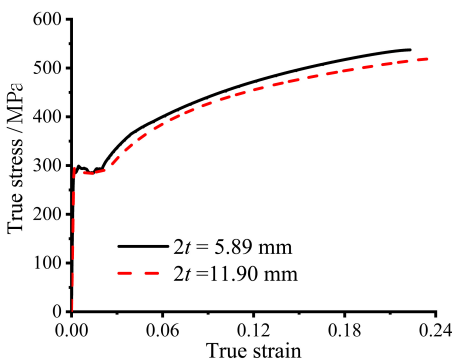

Fig.1 True stress-strain curve of the experimental strip

Tab.1 Material properties of the tested strips

Thickness $2t$ /mm	Young's module E/GPa	Yield stress σ_y/MPa	Ultimate stress σ_u/MPa
5.89	207	296.01	538.67
11.90		283.80	519.72

1.2 Plastic forming process

The concave forming of the strips was conducted on the SKWB-400 forming machine, and the details of the machine can be found in Ref.[16]. Before forming the strip, the heights of lower dies were adjusted and arranged into tool shapes. The strips outlined by red lines were put symmetrically on lower dies, see Fig.2. Then, upper punches were pulled to the pre-determined position (see the left picture in Fig.2). After that, upper punches were driven by hydraulic system and pressed the strip gradually to lower dies until they were close together (see Fig.2 (right)).

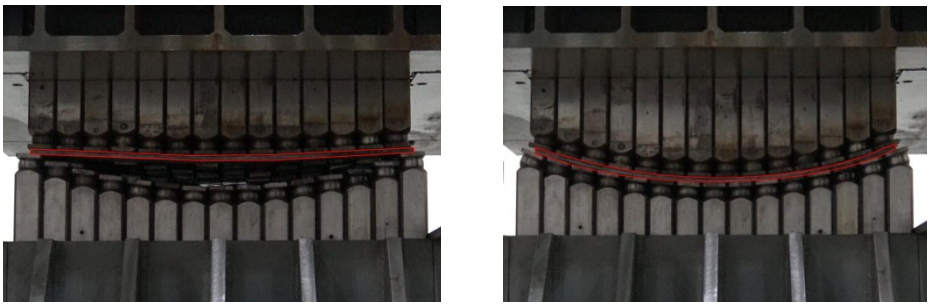

(a) (b)

Fig.2 Concave forming of strips under SKWB-400

According to the dimensions of the SKWB-400 forming machine, the in-plane dimensions of the experimental strips were adopted as 840 mm×50 mm. The tool radius was 1250 mm. Therefore, a forming case is named as R1250T6V, where R1250 denotes that the forming radius is 1250 mm, T6 denotes that the forming strip is 6 mm thick (5.89 mm in fact) and "V" denotes that the strip is to be forming into a concave curve. To provide experimental validations for the theoretical studies, the following cases listed in Tab.2 are chosen to conduct the experiments.

Tab.2 List of concave forming cases of strips

Loading method	Tool radius R/mm	Thickness 2t/mm	Forming cases
Forming into a concave curve	1250	5.89	R1250T6V
		11.90	R1250T12V

The tool shape consisting of the lower dies can be regarded as the shape of the strips before unloading with allowable errors. The final shape of the strip is scanned by the 3D scanner. Then the curve along the mid-width of the upper surface (the surface contacting with the upper punches) is obtained by the Solidworks and AutoCAD, and is adopted as the final curve of the strip presenting in the following analysis.

2 Theoretical analysis of forming process

According to the observations in the experiments of strips' multi-square punch concave forming, the deformation process for strips pressed into flexible lower dies can be divided into two predominant stages, i.e. the elastic-plastic deformation before bottoming and after bottoming. Each stage has its own assumptions and approximations for solving the deformation and the springback in a relatively easy way.

2.1 Elastic-plastic bending before bottoming

Similar to the forming scenario in Ref.[16], each upper punch applies a same load to the strip during the forming process, and every upper punch and lower die can rotate freely to contact with the strip along their normal directions, thus, it is rational to assume that the upper punches exert a uniformly distributed normal load q on the strip. The strip is simply supported by the lower dies at two ends (D and A) along the normal direction at the contact position of the lower dies, and frictions also exist between the upper punches and the strip, as well as between the strip and the lower dies (see Fig.3). The bold solid line is the deformed strip and the dash line represents the friction q_f between the upper punches and the strip.

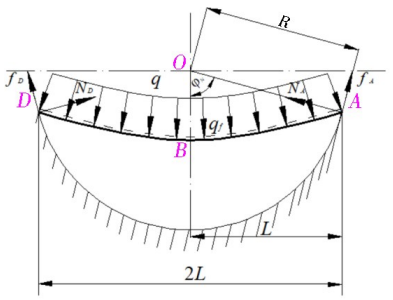

Fig. 3 Schematic of the strip under normally distributed loadings in concave forming

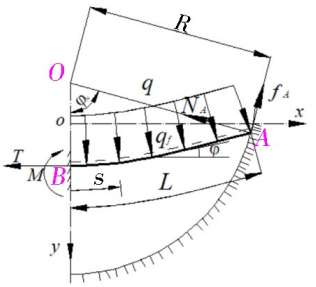

Fig. 4 Elastic-plastic bending of the strip in concave forming

Since the strip and its loading and boundary conditions are symmetrical, a half of the strip is taken for analysis. The coordinate system is established as shown in Fig.4, and the centre (o) of the strip at the flat state is adopted as the origin of the x and y coordinates. For the convenience of calculation, the arc coordinate s is measured from the centre (B) of the deformed strip, and the slope $\varphi(s)$ of the centroid axis of the strip is measured from x axis counter clockwise. The local arc coordinate and the global coordinate satisfy

$$\mathrm{d}x = \cos\varphi(s)\,\mathrm{d}s,\ \mathrm{d}y = -\sin\varphi(s)\,\mathrm{d}s \tag{1}$$

The whole length of the strip is assumed to be constant, thus the right end of the strip (i.e. Point A in Fig.4) will slide along the lower dies during the forming process. The support and the friction at Point A from the lower dies change during the deformation of the strip, but they are always along the normal and tangential directions of the corresponding point on the lower dies, respectively. In addition, the centre of the whole strip, i.e. Point B in Fig.4 (also the left end of the half-length strip), moves vertically during the forming, and the slope is zero at Point B due to the symmetry of the system. Taking Eq.(1) into consideration, the integration of the x and y coordinates of the strip's segment along the half-length strip can be

$$\int_0^L \mathrm{d}x = R\sin\varphi_N = x_A - x_B,\ \int_0^L \mathrm{d}y = y_A - y_B \tag{2}$$

where, y_A and y_B denote the y coordinate of Points A and B on the strip respectively, and L is the half-length of the strip.

The equilibrium equation along the y direction can be expressed as

$$N_A\cos\varphi_N + f_A\sin\varphi_N + \int_0^L q_f\sin\varphi(s)\,\mathrm{d}s = \int_0^L q\cos\varphi(s)\,\mathrm{d}s \tag{3}$$

where, φ_N is the slope of the lower dies at the corresponding point of A of the strip; N_A and f_A are the supporting force and the dynamic friction at Point A of the strip provided by the lower dies respectively, q_f is the dynamic friction between the strip and the upper punches, and the dynamic frictions satisfy

$$f_A = \mu N_A,\ q_f = \mu q \tag{4}$$

where μ is the dynamic friction coefficient between the strip and the punches/dies.

Assuming that the strip has unit width and that its whole extent and thickness are $2L$ and $2t$, respectively, then the following non-dimensional parameters are adopted to describe the entire forming process:

$$\rho = \frac{\sigma_y}{E}\frac{L}{t},\ \lambda = L/R,\ \beta = \frac{\lambda}{\rho} = \frac{E}{\sigma_y}\frac{t}{R},\ \gamma = L/t \tag{5}$$

Substituting Eq.(2) and Eq.(4) into Eq.(3),

$$N_A^* = \frac{2q^*}{3\gamma\lambda}\frac{\sin\varphi_N - \lambda\mu\left(y_B^* - y_A^*\right)}{\cos\varphi_N + \mu\sin\varphi_N} \tag{6}$$

where, $N_A^*=N_A/(2\sigma_y t)$ and $q^*=q/q_e$ denote the non-dimensional supporting force provided by the lower dies at the right end (Point A) of the strip and non-dimensional uniformly distributed normal load from the upper punches respectively, $q_e=3\sigma_y t^2/L^2$ is the maximum elastic uniformly distributed normal load.

Also, the equilibrium equation along the axial direction of the strip at arbitrary position s can be established, and the non-dimensional axial force along the strip can be expresses as in Eq.(7),

$$\begin{aligned} T^*(s^*) = {} & N_A^*\left\{\mu\cos\left[\varphi_N - \varphi(s^*)\right] - \sin\left[\varphi_N - \varphi(s^*)\right]\right\} + \frac{2q^*}{3\gamma}\left\{\left[\mu\cos\varphi(s^*) - \sin\varphi(s^*)\right]\times\right. \\ & \left.\left[x_A^* - x^*(s^*)\right] + \left[\mu\sin\varphi(s^*) + \cos\varphi(s^*)\right]\left[y^*(s^*) - y_A^*\right]\right\} \end{aligned} \tag{7}$$

where, $T^*(s^*)= T(s)/(2\sigma_y t)$ is non-dimensional axial force, $x_A^*= x_A/L=\sin\varphi_N/\lambda$ and $y_A^*=y_A/L$ denote x and y coordinates of Point A in Fig.4, and $s^*=s/L$ is the non-dimensional arc coordinate in Fig.4.

The bending moment at arbitrary position s^* can be expressed non-dimensionally by the equilibrium equation of the bending moment of the strip,

$$\begin{aligned} M^*(s^*) = {} & \mu q^*\int_{s^*}^1\left\{\sin\varphi(\tau)\left[x^*(\tau) - x^*(s^*)\right] - \cos\varphi(\tau)\left[y^*(s^*) - y^*(\tau)\right]\right\}\mathrm{d}\tau + \\ & 3\gamma N_A^*\left\{\left(\cos\varphi_N + \mu\sin\varphi_N\right)\left[x_A^* - x^*(s^*)\right] + \left(\sin\varphi_N - \mu\cos\varphi_N\right)\left[y^*(s^*) - y_A^*\right]\right\} - \\ & q^*\left\{\left[y^*(s^*) - y_A^*\right]^2 + \left[x_A^* - x^*(s^*)\right]^2\right\} \end{aligned} \tag{8}$$

where $M^*(s^*) = 3M(s)/(2\sigma_y t^2)$ is non-dimensional moment.

From the static tensile tests of the strip in Fig.1, the material of the strip is strain-hardening. However, the strain of the forming cases in this paper are all small, thus the elastic-perfectly-plastic relationship is applied to approximate the material characteristics of the strip.

It is assumed that the rectangular section of the strip remains unchanged. The non-dimensional curvature of the elastic-perfectly-plastic strip under the combined loading including bending moment and axial force[6] can be expressed as Eq.(9),

$$\kappa^* = \begin{cases} M^*, & 0 \leqslant M^* \leqslant 1 - T^* \\ 4\left(1 - T^*\right)/\left[3 - M^*/(1 - T^*)\right]^2, & 1 - T^* < M^* \leqslant \left(2T^* + 1\right)\left(1 - T^*\right) \\ 1/\sqrt{3\left(1 - T^{*2}\right) - 2M^*}, & -2T^{*2} + T^* + 1 < M^* < \dfrac{3}{2}\left(1 - T^{*2}\right) \end{cases} \tag{9}$$

where, $\kappa^*=\kappa/\kappa_y$ and $\kappa_y=\sigma_y/(Et)$; M^* and T^* are non-dimensional moment and axial force calculated by Eq.(7) and Eq.(8), respectively. It should be noted that Eq.(9) is only applied for small strain scenario with elastic-perfectly-plastic constitutive relationship.

Substituting Eq.(7) and Eq.(8) into Eq.(9), the curvature of arbitrary position on the strip can be obtained, and the slope of the corresponding position can also be gained by integrating the curvature along the strip from Point B to the position,

$$\varphi(s^*) = \int_0^{s^*}\rho\,\kappa^*(s^*)\,\mathrm{d}s^* \tag{10}$$

where the boundary condition at Point B, i.e. the slope is zero, is implied.

Since the right end (Point A) of the strip slides along the lower dies, the direction of the supporting force (φ_N) at Point A can be updated through Eq.(11),

$$\sin\varphi_N = \lambda\int_0^1 \cos\varphi\left(s^*\right)\mathrm{d}s^* \tag{11}$$

Once the direction of the supporting force is determined, the position (x and y coordinates) of A is obtained. According to the geometric relationship and Eq.(2), the y coordinate of Point B can be updated,

$$y_B{}^* = \int_0^1 \sin\varphi\left(s^*\right)\mathrm{d}s^* + \left(\cos\varphi_N - \sqrt{1-\lambda^2}\right)/\lambda \tag{12}$$

and the deformation profile of the strip can be acquired through

$$x^*\left(s^*\right) = \int_0^{s^*} \cos\varphi\left(s^*\right)\mathrm{d}s^*,\ y^*\left(s^*\right) = y_B{}^* - \int_0^{s^*} \sin\varphi\left(s^*\right)\mathrm{d}s^* \tag{13}$$

With the increase of the loading q, the strip can bottom. Assuming that Point B is the first point (except Point A) that contacts the lower dies during the forming process, it satisfies

$$\left(y_B{}^*\right)_{\text{bottom}} = \left(1-\sqrt{1-\lambda^2}\right)/\lambda \tag{14}$$

2.2 Elastic-plastic bending with one-point bottoming

As mentioned in Section 2.1, the strip will bottom when the loading increases, in the case of which the supporting and the boundary conditions of the strip can be quite different. Due to the arbitrariness of the forming shape and the complexity of the loading condition, the strip can bottom at different positions on the lower dies. In this section, a special case, where the left end of the strip (Point B) exactly bottoms before other part of the strip bottoms as shown in Fig.5, is taken as an example to elaborate the forming mechanism of the strip in one-point bottoming cases. For other cases where some point between Point A and Point B bottoms, the analysis is similar.

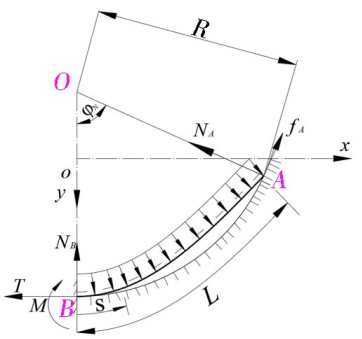

Fig. 5 One-point bottoming of the strip in concave forming

For the case presented in Fig.5, the force equilibrium equations in the normal and axial directions and the bending equilibrium equation can be established non-dimensionally,

$$N_A{}^* = \frac{2q^*}{3\gamma\lambda}\frac{\sin\varphi_N - \lambda\mu\left(y_B{}^* - y_A{}^*\right)}{\cos\varphi_N + \mu\sin\varphi_N} - \frac{N_B{}^*}{\cos\varphi_N + \mu\sin\varphi_N} \tag{15}$$

$$\begin{aligned} T^*\left(s^*\right) = {} & N_A{}^*\left\{\mu\cos\left[\varphi_N - \varphi\left(s^*\right)\right] - \sin\left[\varphi_N - \varphi\left(s^*\right)\right]\right\} + \frac{2q^*}{3\gamma}\left\{\left[\mu\cos\varphi\left(s^*\right) - \sin\varphi\left(s^*\right)\right]\times\right. \\ & \left.\left[x_A{}^* - x^*\left(s^*\right)\right] + \left[\mu\sin\varphi\left(s^*\right) + \cos\varphi\left(s^*\right)\right]\left[y^*\left(s^*\right) - y_A{}^*\right]\right\} \end{aligned} \tag{16}$$

$$\begin{aligned} M^* = {} & \mu q^*\int_{s^*}^1 \left\{\sin\varphi(\tau)\left[x^*(\tau) - x^*(s^*)\right] - \cos\varphi(\tau)\left[y^*(s^*) - y^*(\tau)\right]\right\}\mathrm{d}\tau + \\ & 3\gamma N_A{}^*\left\{\left(\cos\varphi_N + \mu\sin\varphi_N\right)\left[x_A{}^* - x^*\left(s^*\right)\right] + \left(\sin\varphi_N - \mu\cos\varphi_N\right)\left[y^*\left(s^*\right) - y_A{}^*\right]\right\} - \\ & q^*\left\{\left[y^*(s^*) - y_A{}^*\right]^2 + \left[x_A{}^* - x^*(s^*)\right]^2\right\} \end{aligned} \tag{17}$$

It can be easily concluded that the curvature at Point B of the strip is larger than the curvature of the lower dies at the corresponding position when the bottoming occurs. After bottoming, the axial force and bending moment as well as the strip's curvature decrease due to the support at Point B, i. e., the unloading occurs at Point B and the nearby part, while the part of the strip far away from Point B is still in the state of loading.

Eq.(9) is only applied to the curvature calculation when the strip is loaded from the flat state. However, the strip has initial deformation after bottoming, and some part of the strip is unloaded while other part will be loaded continuously. For the loading part, the curvature can still be obtained by Eq.(9) with the curvature κ_0^* in the previous step. For the unloading and the reverse loading part, the linear elastic unloading assumption is adopted, and the variation of the strip's stiffness in reverse loading and the Bauschinger effect are ignored. Then the curvature of the strip can be obtained by the superposition of the original curvatures and moments[21],

$$\kappa^* = \begin{cases} \kappa_0^* - M_0^* + M^*, & 0 \leqslant M^* \leqslant M_{\max}^* \\ \kappa_0^* - M_0^* + M^*, & T^* - 1 \leqslant M^* < 0 \\ \kappa_0^* - M_0^* - 4\left(1 - T^*\right)/\left[3 + M^*/\left(1 - T^*\right)\right]^2, & \left(2T^* + 1\right)\left(T^* - 1\right) \leqslant M^* < T^* - 1 \\ \kappa_0^* - M_0^* - 1/\sqrt{3\left(1 - T^{*2}\right) + 2M^*}, & \dfrac{3}{2}\left(T^{*^2} - 1\right) < M^* < \left(2T^* + 1\right)\left(T^* - 1\right) \end{cases} \tag{18}$$

where κ_0^* and M_0^* are the non-dimensional curvature and non-dimensional bending moment in the previous step respectively, $M_{\max}^*$ denotes the maximum non-dimensional bending moment during the whole forming process, and the corresponding curvature is also the maximum deforming curvature. It should be noted that the maximum bending moment and the maximum deforming curvature are different at different positions of the strip, thus the loading-unloading history should be considered at the analysed point of the strip when applying Eq.(18).

Obviously, the strip is over-determined after bottoming, and extra compatibility equation should be introduced to solve Eqs.(15)-(17). The deformation of the strip leads to the change of the strip′s shape (curvature), the slide of the right end (Point A) of the strip and the vertical movement of the central point (Point B) of the strip. Since the bottoming point (Point B) of the strip is supported by the lower dies after bottoming, there is no more vertical movement at Point B, i.e.,

$$\Delta y_B^* = 0 \text{ or } y_B^* = \left(y_B^*\right)_{\text{bottom}} = \left(1 - \sqrt{1 - \lambda^2}\right)/\lambda \tag{19}$$

In the analysis in Section 2.1, it is assumed that φ_N remains unchanged in a loading step. Once the loading is determined, the forming curvature can be obtained by taking the bending moment and the axial force into Eq.(9). Then, the slope can be integrated through Eq.(10). Finally, the movement of Point B can be gained by Eq.(12). However, the supporting force (N_B^*) provided by the lower dies is unknown after the strip bottoms. The deformation of the strip will be solved through the following iterative steps:

(i) Suppose an initial $N_{B(0)}^*$;

(ii) Substitute the supposed $N_{B(0)}^*$ into Eq.(16) and Eq.(17) to obtain the axial force $T^*$and the bending moment $M^*$of the strip, respectively;

(iii) Substitute $T^*$and M^* into Eq.(18) to gain the curvature κ^*;

(iv) Integrate κ^*along the strip to obtain the slope φ by Eq.(10);

(v) Integrate φ along the strip to φ_N by Eq.(11);

(vi) Solve y_B^* through Eq.(14);

(vii) Judge whether Eq.(19) is satisfied:

- If it is satisfied, solve the deformation profile of the strip by Eq.(13);
- If not, modify $N_{B(0)}^*$ and repeat Steps (ii)–(vii) until Eq.(19) is satisfied.

As the forming progresses, the unloading occurs at Point B and propagates to the nearby parts, and the curvature reduces due to the combined loading from the upper punches and the support of the lower dies, while the bending moments and the curvature of other parts of the strip increase with the increase of q^*, thus, the bottoming of two or more points will occur with the forming going.

2.3 Elastic-plastic bending with two- or more-points bottoming

With the increase of the loading, the strip can bottom at two or more points. Following the analysis in Section 2.2, when one more point bottoms, i.e., Point C in Fig.6, a new supporting force (N_C) is introduced at the bottoming Point C. The coordinates of the new bottoming Point C is equal to the ones of the corresponding point on the lower dies,

$$x^*\left(s_C^*\right) = x_R^*\left(s_C^*\right),\ y^*\left(s_C^*\right) = y_R^*\left(s_C^*\right) \tag{20}$$

where x_R^* and y_R^* are the non-dimensional coordinates on the lower dies along the x and y axes respectively, and s_C^* is the non-dimensional arc coordinate of the bottoming Point C.

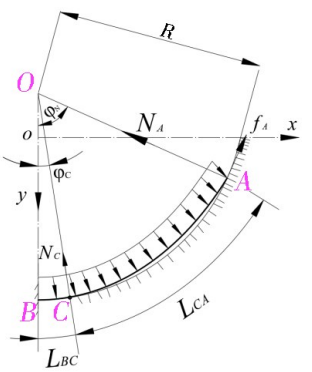

Fig.6 Two-points bottoming of the strip in concave forming

The calculation of the strip's deformation with two-points bottoming is similar to that in one-point bottoming. For the segment BC, replace N_A^*, x_A^*, y_A^*, φ_N in Eqs.(15)–(17) with N_C^*, x_C^*, y_C^*, φ_C and the integration interval alters from the whole strip's length to $L_{BC}^* = L_{BC}/L$ that meets,

$$L_{BC}^* = s_C^*,\ L_{CA}^* = 1 - s_C^* \tag{21}$$

Then the non-dimensional bending moment, axial force and the curvature of the segment BC can be obtained following the analysis process in Section 2.1, and the direction of the supporting force (φ_C) at Point C can be gained through

$$\sin\varphi_C = \lambda \int_0^{L_{BC}^*} \cos\varphi\left(s^*\right) \mathrm{d}s^* \tag{22}$$

It should be noted that the slope of the strip is in the same direction as the supporting force provided by the lower dies at Point C, since the strip bottoms at this point. Once the direction of the supporting point is determined, the position of the new bottoming point is also determined. For the segment CA, the analysis is similar while the left end changes from Point B to Point C where there is no rotation during the following analysis. Similarly, the bottoming strip is also over-determined, and extra compatibility equation should be introduced, i.e., the new end Point C does not move due to the support of the lower dies, and it satisfies the compatibility equation,

$$y_C^* = \left(\cos\varphi_C - \sqrt{1 - \lambda^2}\right)/\lambda \tag{23}$$

The procedure for solving the deformation of the strip after two-points bottoming is similar to the process in Section 2.2. An arbitrary $N_{C(0)}^*$ is first supposed to obtain the distribution of the axial

force and the bending moment. Then the curvature of the segment CA can be solved through Eq.(18) if unloading occurs, and the slope can be gained by integrating the curvature from Point C to the corresponding point whose arc coordinate is s^*,

$$\varphi(s^*) = \int_C^{s^*} \rho\,\kappa^*(s^*)\,\mathrm{d}s^* + \varphi_C \tag{24}$$

The supporting direction (φ_N) at the right end (Point A) of the strip can be updated,

$$\sin\varphi_N = \lambda \int_C^A \cos\varphi(s^*)\,\mathrm{d}s^* + \sin\varphi_C \tag{25}$$

and the y coordinate of Point C can be updated according to the position of Point A,

$$y_C{}^* = \int_C^A \sin\varphi(s^*)\,\mathrm{d}s^* + \left(\cos\varphi_N - \sqrt{1-\lambda^2}\right)/\lambda \tag{26}$$

Judge whether the compatibility condition in Eq.(23) is satisfied. If not, modify $N_{C(0)}{}^*$ and repeat the above process until Eq.(23) is satisfied. The deformation of the segment CA can also be obtained through Eq.(27) after $N_C{}^*$ is determined.

$$x^*(s^*) = \int_{s_C{}^*}^{s^*} \cos\varphi(s^*)\,\mathrm{d}s^* + \sin\varphi_C/\lambda,\ y^*(s^*) = y_C{}^* - \int_{s_C{}^*}^{s^*} \sin\varphi(s^*)\,\mathrm{d}s^* \tag{27}$$

With the increase of the loading force q, more points bottoming will occur, and the analysis can also refer to the procedure in this section with corresponding boundary conditions and the integral interval of the strip.

2.4 Springback after unloading

When the loading finishes, the strip is unloaded and springs back due to the release of the elastic energy stored in the strip. The elastic softening is ignored in the paper, i.e., the unloading is linearly elastic, and the Young's module in the unloading process is equal to the one in the loading process. Thus, the final curvature ($\kappa_F{}^*$) of the strip after unloading can be obtained by subtracting the final moment $M_F{}^*$ from the curvature ($\kappa_b{}^*$) of the strip before unloading,

$$\kappa_F{}^* = \kappa_b{}^* - M_F{}^* = \begin{cases} 0, & 0 \leqslant M^* \leqslant 1 - T^* \\ 4\left(1 - T_F{}^*\right)/\left[3 - M_F{}^*/\left(1 - T_F{}^*\right)\right]^2 - M_F{}^*, & 1 - T^* < M^* \leqslant (1 - T^*)(1 + 2T^*) \\ \left[3\left(1 - T_F{}^{*2}\right) - 2M_F{}^*\right]^{-1/2} - M_F{}^*, & (1 - T^*)(1 + 2T^*) < M^* < 1.5\left(1 - T^{*2}\right) \\ \kappa_0{}^* - M_0{}^*, & T^* - 1 \leqslant M^* \leqslant M_{\max}{}^* \\ \kappa_0{}^* - M_0{}^* - 4\left(1 - T_F{}^*\right)/\left[3 + M_F{}^*/\left(1 - T_F{}^*\right)\right]^2 - M_F{}^*, & (2T^* + 1)(T^* - 1) \leqslant M^* < T^* - 1 \\ \kappa_0{}^* - M_0{}^* - 1/\sqrt{3\left(1 - T_F{}^{*2}\right) + 2M_F{}^*} - M_F{}^*, & 1.5\left(T^{*2} - 1\right) < M^* < (2T^* + 1)(T^* - 1) \end{cases} \tag{28}$$

where, $M_F{}^*$ is the non-dimensional bending moment of the strip before unloading, i.e., the final bending moment; $T_F{}^*$ is the non-dimensional axial force before unloading, i.e., the final axial force; and other parameters have the same meaning as before.

It can be seen from Eq.(28) that the final curvature of the strip depends on the curvature of the mould (consisting of lower dies), the final bending moment, the final axial force of the strip and the deformation history. During the forming process, the axial forces of arbitrary points of the strip are not always the same, and reverse bending exists in some part of the strip, thus, the final profile of the strip in concave forming is not a curve with constant curvature, which is different from the cases

in convex forming.

After obtaining the final curvature of the strip by Eq.(28), the slope of the strip can be integrated through

$$\varphi_{\mathrm{F}}(s^*)=\int_0^{s^*}\rho\,\kappa_{\mathrm{F}}{}^*(s^*)\,\mathrm{d}s^* \tag{29}$$

and the final deformation profile after unloading can be gained through

$$x_{\mathrm{F}}{}^*(s^*)=\int_0^{s^*}\cos\varphi_{\mathrm{F}}(s^*)\,\mathrm{d}s^*,\ y_{\mathrm{F}}{}^*(s^*)=(y_{\mathrm{B}}{}^*)_{\mathrm{F}}-\int_0^{s^*}\sin\varphi_{\mathrm{F}}(s^*)\,\mathrm{d}s^* \tag{30}$$

It should be noted that there is no need to divide the strip into different segments according to its supporting conditions, since all loads are removed and the final profile of the strip only depends on the final curvature.

3 Results and discussions

3.1 Experimental validations

The experimental results of the cases in Tab.2 are adopted to verify the accuracy of the theoretical model. As stated in Section 2.2, the profile of the strip before unloading in the experiments can be assumed as equal to the shape of the lower dies, and it can be expressed in Eq.(31) for concave forming with constant curvature according to the coordinate system in Fig.4. The material properties of the strip in the theoretical calculation are the same as those presented in Tab.1. The profile of the strip before unloading calculated through the theoretical model proposed in this paper will firstly be compared with the curve presented by Eq.(31) to ensure that the strip is indeed pressed to the lower dies with allowable shape errors. Then, the final profile of the strip calculated by the theoretical model as proposed in this paper will be compared with the experimental results, as seen in Fig.7.

$$y=\sqrt{R^2-x^2}-\sqrt{R^2-L^2} \tag{31}$$

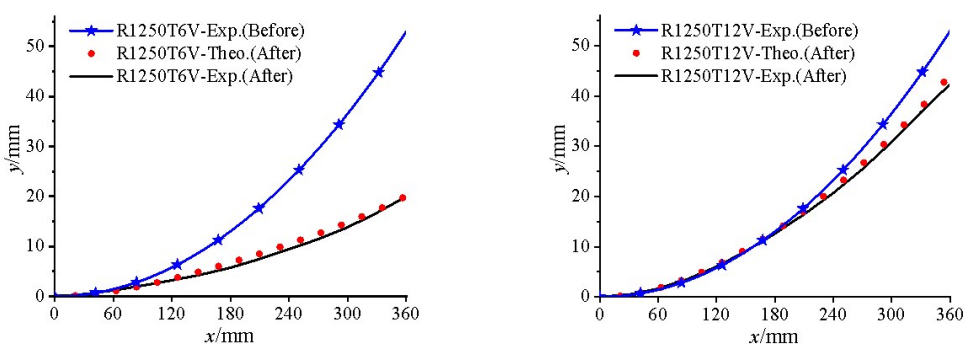

(a) R1250T10V (b) R1250T12V

Fig.7 Theoretical and experimental profile of the strip after springback

In Fig.7, the analytical results calculated by the proposed method are shown by the red dots, while the experimental one is presented by the black curve, and the profile before unloading is described by a blue curve with asterisk. The profile calculated through the theoretical model after springback agrees well with the experimental results, demonstrating the accuracy of the model in predicting the springback of the strip in multi-square punch concave forming process.

3.2 Profiles and loads evolution

The strip is formed to the lower dies with the load provided by the upper punches, and generic formula that is applied to predict the springback is highly dependent on the shape before unloading. Thus, whether the machine is capable of forming the strip to the designed shape matters and has a great significance for the springback prediction. The analytical method is explored step by step along the deformation history, so the loading and the profile can be easily obtained through the proposed method. The profiles and loads during the forming process in Case R1250T6V and Case R1250T12V are illustrated in Fig.8 and Fig.9 respectively.

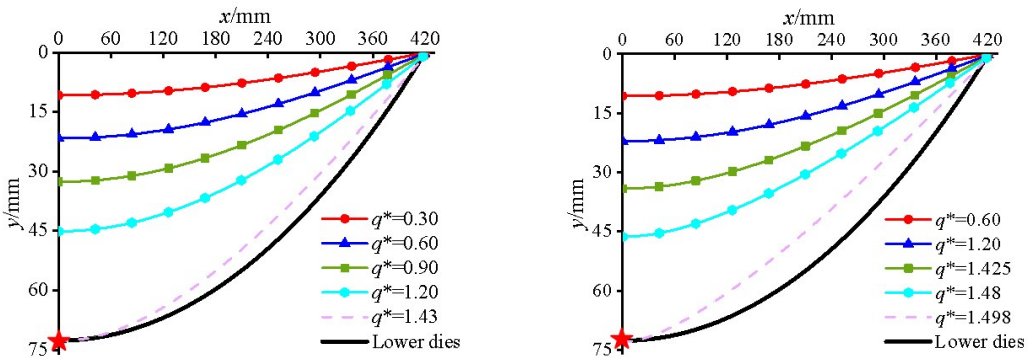

(a) R1250T6V (b) R1250T12V

Fig.8 Profiles of the strip before the first bottoming

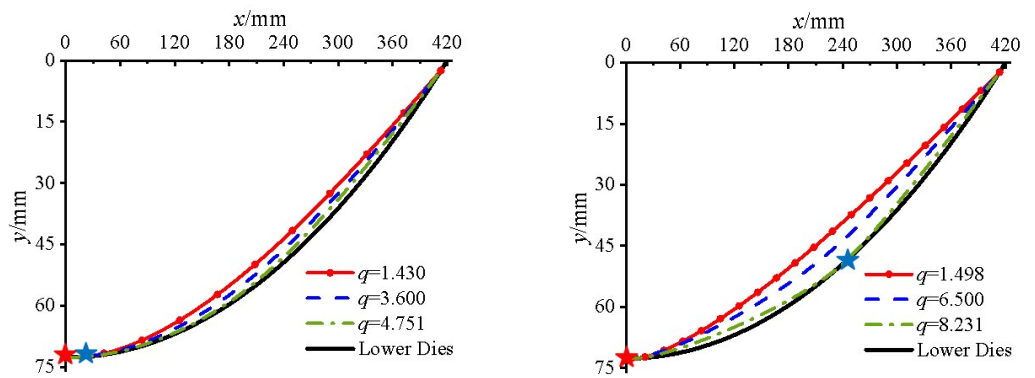

(a) R1250T6V (b) R1250T12V

Fig.9 Profiles of the strip before the second bottoming

Fig.8 shows the profiles of the strip before the first bottoming while the bold black curve represents the lower dies, and the corresponding loads q^* are given in the legends. During this process, the applied load is relatively small to form the strip, but it is non-dimensioned by $q_e=3\sigma_y t^2/L^2$ and it induces large deformation while approaching to 1.5, which is the upper limit load of the elastic-perfectly-plastic strip. The pink dash curves in Fig.8 illustrate the profile of the strip when the first bottoming happens at the middle of the strip due to the symmetry, and the bottoming point marked with a red asterisk. Although the non-dimensional loading is similar in Case R1250T6V (i.e. $q^*=1.43$) and in Case R1250T12V (i.e. $q^*=1.498$), it should be noted that the q_e is different in these two cases, and the forming capacity for the first bottoming applied in the Case R1250T12V is at least four times larger than that in the Case R1250T6V actually.

Fig.9 shows the profiles of the strip and the corresponding loads before the second bottoming. The bold black curve still represents the lower dies, the red curve with dots is the profile when the first bottoming happens and the olive dash-dot curve indicates the profile when the second bottoming takes place. During this process, the applied loads increase largely compared with the ones before the first bottoming. Also, the bottoming points marked by a blue asterisk in Fig.9 are not necessarily symmetrically positioned. The second bottoming point is closely right to the first bottoming point in Case R1250T6V, while it is nearly at the middle of the half-strip in Case R1250T12V. Besides, the forming load for the second bottoming applied in the Case R1250T12V is nearly eight times larger than that in the Case R1250T6V.

The forming process does not end as shown in Fig.9, and the forming load should continue to increase significantly such that the strip can be deformed to the designed shape. The advantage of the proposed analytical method is that the forming load needed for the certain case can be pre-calculated in case of the insufficient manufacturing capacity of the forming machine.

3.3 Effect of forming approaches

The deformation and the springback of the strip are comprehensively affected by the thickness, the forming curvature and the forming approaches in concave forming. While the influence of the thickness and the forming curvature are discussed in Ref.[16], no more discussion will be further presented for these two factors. To investigate the effect of the forming approaches alone, the following four forming cases listed in Tab.3 are conducted, and no friction and no elongation are considered in all forming cases.

Tab.3 Forming cases of different forming approaches

Forming cases	Thickness $2t$/mm	Forming curvature R/mm	Forming approach
R1250T6V	6	1250	concave(V)
R1250T6A			convex (A)
R1250T12V	12		concave(V)
R1250T12A			convex (A)

The strips in these cases are all from the same steel as in Tab.1, and the length is 420 mm and the forming curvature is 1250 mm. While for each forming thickness, the profile of the strip after springback formed by two different approaches are compared in Fig.10.

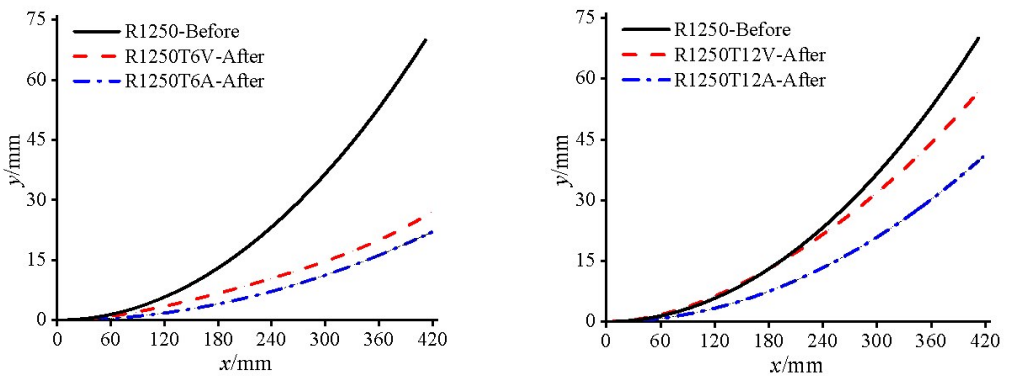

(a) R1250T6V and R1250T6A　　(b) R1250T12V and R1250T12A

Fig.10 Comparisons of the strip's profiles after springback in concave (V) and convex (A) forming

In Fig.10, the black solid curve denotes the profile of the strip before springback, the red dash curve presents the profile of the strip after springback in concave forming, while the blue dash-dot curve is the profile of the strip after springback in convex forming. It can be seen from Fig.10 that the springback in concave forming is smaller than the one in convex forming, which means that the partial unloading in concave forming can restrain the springback of the strip. To further reveal the inner mechanism, the non-dimensional $M^*-\kappa^*$ curves at different positions on the strip in R1250TjV/A (j=6 and 12) cases are illustrated in Fig.11, where the non-dimensional arc coordinate s^* is measured in the local coordinate system in Fig.4.

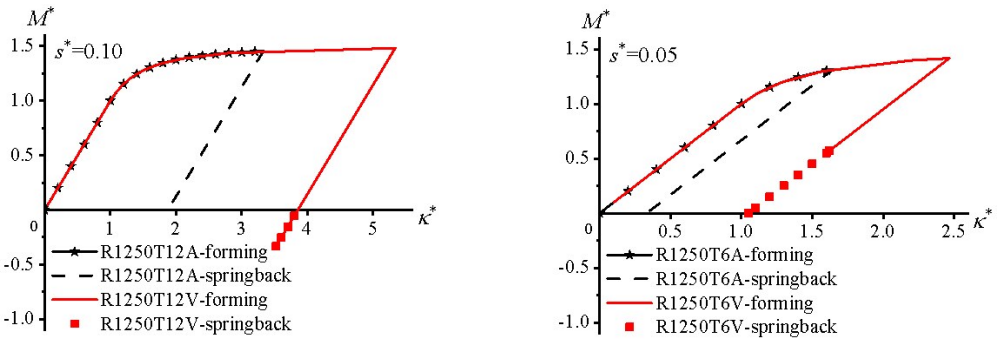

(a) R1250T12V and R1250T12A (b) R1250T6V and R1250T6A

Fig.11 Non-dimensional $M^*-\kappa^*$ curves at different s^* on the strip in concave and convex cases

In the forming stage when q^* increases, the non-dimensional bending moment M^* and non-dimensional curvature κ^* increase continuously before the strip wraps (in convex forming cases) or bottoms (in concave forming cases), referring to the initial ascent in Fig.11. The curvature of the strip at the wrapping point is equal to the one of lower dies at the corresponding point when the strip begins to wrap the lower dies in convex forming. After the strip wraps the lower dies, the wrapping part of the strip will not deform due to the restraints from the upper punches and lower dies, i.e. the curvature of the wrapping part of the strip before unloading is equal to the lower die. Ignoring the material softening, the unloading of the strip is linearly elastic (black dash in Fig.11).

However, the curvature of the strip at the bottoming point is larger than the one of the lower dies at the corresponding point when the strip bottoms in concave forming, to make sure that the bottoming point is the only one point nearby that contacts the lower dies. After the strip bottoms, the bending moment and the curvature of the part of the strip reduce even though the loading q^* increases, which seems that "unloading" happens to the bottoming part of the strip. Thus, the calculation of the strip needs to be divided into the two parts, and the relationship between the non-dimensional bending moment and the curvature evolves as Eq.(18) until the loading ends. The unloading of the strip is still linearly elastic and the final curvature of the strip after unloading is calculated through Eq.(28).

In general, although the curvatures of the lower dies, i.e., the designed mould shape, in two forming approaches are the same, the maximum forming curvature of the strip in concave forming is larger than the one in convex forming during the whole forming process to ensure that the strip can

bottom, thus, the final curvature of the strip in concave forming is larger than the one in convex forming. In addition, the curvature of the strip at the wrapping point is always equal to the lower dies in convex forming, thus, the curvatures before unloading are the same at the wrapping part of the strip. However, the forming scenario is quite different in concave forming, where nearly every point′s curvature on the strip is different, as seen in Fig.12.

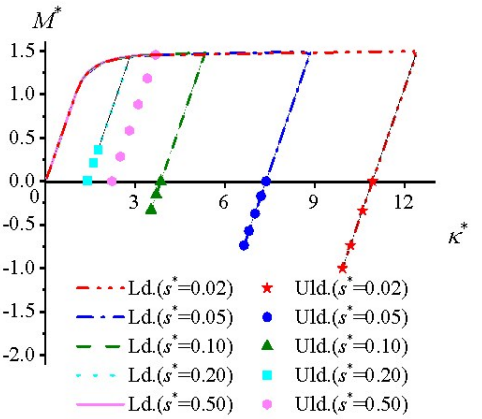

Fig.12 Non-dimensional M^*-κ^* curves at different s^* in Case R1250T12V

The curves in Fig.12 represent the moment-curvature relationship of different points (s*=0.02, 0.05, 0.10, 0.20, 0.50) on the strip during the forming process. According to the coordinate system in Fig.4, the smaller the s* is, the closer the point is to the middle point of the strip, i.e., the Point B (where the first bottoming happens). The maximum forming curvature decreases as the investigated point is away from Point B, while the maximum forming curvature further increases as the point (e.g. s*=0.50) is approaching the second bottoming point, i.e., nearly the middle of half-strip in Fig.9(b). Furthermore, the larger the maximum forming curvature is, the larger the final curvature after springback will be, as described by symbols in Fig.12. In general, two forming approaches result in diverse maximum forming curvatures, and the final curvature of the strip in concave forming is larger than the one in convex forming.

4 Concluding remarks

The forming and springback of the strip in multi-square punch concave forming is explored experimentally in this paper, setting a springback database to provide validations for the theoretical analysis of the strip. A simplified theoretical model is established to reproduce the forming and springback behaviour of the strip and to investigate the inner deforming mechanism, and good agreements between the analytical and experimental results are achieved, validating the accuracy of the theoretical work. Based on the proposed formulae, the forming history and the required loads can be easily gained, which can provide suggestions on whether the forming machine is capable of manufacturing the material into the designed shape and controlling the forming load in a proper range for the designed case. The effect of the forming approaches on the springback is discussed, and the results show that the springback in convex forming is larger than the one in concave forming due to the existence of the partial unloading process of the strip in concave forming. Although the springback is smaller in concave forming compared with the one in convex forming, the uneven bottoming could lead to wrinkles compared with the wrapping approach in convex forming. Thus, the proposed method can be applied to perform the forming process and to modify the loading and the designed shape easily before practical manufacturing, further reducing the cost and improving the forming efficiency.

Acknowledgement

The authors appreciate the support of the general project of the National Natural Science Foundation of China (Grant No. 52201378). The authors also appreciate Mr. Lin Zexin and Mr. Xu Lijun , for their help and support to the experimental studies carried out in the paper.

References

[1] Qi L, Ge C, Huang J, et al. Experimental research on mechanism of hull plates curved forming by a clean energy source[J]. Journal of Ship Mechanics, 2021, 25(12): 1729-1743.

[2] Li M, Liu Y, Su S, et al. Multi-point forming: A flexible manufacturing method for a 3-d surface sheet[J]. Journal of Materials Processing Technology, 1999, 87(1-3): 277-280.

[3] Su S, Hu Y, Wang C. The key technology research about 3D CNC bending machine and experimental verification[J]. Journal of Coastal Research, 2015 (73 (10073)): 584-588.

[4] Xu L Z, Shen W, Yan R. Predictive and control models of the spring-back in thick hull plate forming[J]. International Journal of Material Forming, 2019, 12: 603-614.

[5] Shen W, Yan R, Li S, et al. Spring-back analysis in the cold-forming process of ship hull plates[J]. The International Journal of Advanced Manufacturing Technology, 2018, 96: 2341-2354.

[6] Yu T X, Zhang L. Plastic bending: Theory and applications[M]. World Scientific, 1996.

[7] Zhang L C, Lin Z. An analytical solution to springback of sheet metals stamped by a rigid punch and an elastic die[J]. Journal of Materials Processing Technology, 1997, 63(1-3): 49-54.

[8] Tari H, Kinzel G L, Mendelsohn D A. Cartesian and piecewise parametric large deflection solutions of tip point loaded Euler-Bernoulli cantilever beams[J]. International Journal of Mechanical Sciences, 2015, 100: 216-225.

[9] Satō K. Large deflection of a circular cantilever beam with uniformly distributed load[J]. Ingenieur-Archiv, 1959, 27: 195-200.

[10] Beléndez T, Pérez-Polo M, Neipp C, et al. Numerical and experimental analysis of large deflections of cantilever beams under a combined load[J]. Physica Scripta, 2005, 2005(T118): 61.

[11] Elishakoff I. Controversy associated with the so-called "follower forces": Critical overview[J]. Applied Mechanics Reviews, 2005, 58(2): 117-142.

[12] Nallathambi A K, Rao C L, Srinivasan S M. Large deflection of constant curvature cantilever beam under follower load[J]. International Journal of Mechanical Sciences, 2010, 52(3): 440-445.

[13] Liang Q, Zhu L. Springback prediction and compensation of elastic-perfectly plastic strip in multi-square punch forming [J]. Advances in Applied Mathematics and Mechanics, 2020, 12(4): 1057-1078.

[14] Shvartsman B S. Large deflections of a cantilever beam subjected to a follower force[J]. Journal of Sound and Vibration, 2007, 304(3-5): 969-973.

[15] Shvartsman B S. Direct method for analysis of flexible cantilever beam subjected to two follower forces[J]. International Journal of Non-Linear Mechanics, 2009, 44(2): 249-252.

[16] Zhu L, Liang Q, Yu T X, et al. Experimental and theoretical study of constant curvature multi-square punch forming process of strips under follower load[J]. International Journal of Mechanical Sciences, 2019, 156: 462-473.

[17] Coubrough G J, Alinger M J, Van Tyne C J. Angle of contact between sheet and die during stretch-bend deformation as determined on the bending-under-tension friction test system[J]. Journal of Materials Processing Technology, 2002, 130: 69-75.

[18] Brunet M, Morestin F, Godereaux S. Nonlinear kinematic hardening identification for anisotropic sheet metals with bending-unbending tests[J]. Journal of Engineering Materials & Technology, 2001, 123(4): 378-383.

[19] Eggertsen P A, Mattiasson K. On the modelling of the bending-unbending behaviour for accurate springback predictions[J].

International Journal of Mechanical Sciences, 2009, 51(7): 547-563.

[20] Pandit D, Patel B N. On numerical moment-curvature relationship of a beam[J]. Sādhanā, 2022, 47(1): 27.

[21] Pascon J P. Numerical analysis of highly deformable elastoplastic beams[J]. Latin American Journal of Solids and Structures, 2015, 12: 1595-1615.

考虑部分卸载效应的多压头凹形成形及回弹预测

梁棋钰[1,2], 张 龙[1,2,3], 朱 凌[1,2,3]

(1. 高性能船舶技术教育部重点实验室(武汉理工大学), 武汉 430063; 2. 武汉理工大学 船海与能源动力工程学院, 武汉 430063; 3. 武汉理工大学 威海研究院, 山东 威海 264309)

摘要: 为了进一步探索考虑部分卸载效应的板条多压头成形机理和回弹特性,本文在船舶数控弯板机上开展一系列板条凹形成形试验。首先建立板条成形的理论模型,分析板条在凹形成形中的变形机理和回弹特性,并与实验结果对比,验证该模型的准确性;然后在该理论模型基础上,进一步分析板条的变形历史和加载情况,探索不同加工工况所需的船舶数控弯板机加工能力;此外还分析成形方式对板条回弹的影响,结果表明,凸形成形的板条回弹量大于凹形成形的回弹量。

关键词: 多压头成形; 跟随载荷; 弹塑性变形; 部分卸载; 回弹预测

中图分类号: U661.4 **文献标识码:** A

基金项目: 国家自然科学基金资助项目(52201378); 武汉理工大学威海研究院开放基金(WHYJY-KJ2021-008)

作者简介: 梁棋钰(1993-),女,武汉理工大学讲师,硕士生导师;

张 龙(2000-),男,硕士研究生;

朱 凌(1962-),男,武汉理工大学教授,博士生导师。